Radiation losses in planar photonic crystals: two-dimensional representation of hole depth and shape by an imaginary dielectric constant

Rolando Ferrini and Romuald Houdré

Institut de Photonique et d'Electronique Quantique, Ecole Polytechnique Fédérale de Lausanne, CH-1015 Lausanne, Switzerland

Henri Benisty

Laboratoire de Physique de la Matiére Condensée, Ecole Polytechnique, F-91128 Palaiseau Cedex, France

Min Qiu

Department of Microelectronics and Information Technology, Royal Institute of Technology, Electrum 229, S-16440 Kista, Sweden

Jürgen Moosburger

Technische Physik, University of Würzburg, Am Hubland, D-97074 Würzburg, Germany

Received May 3, 2002; revised manuscript received August 9, 2002

Waveguide modes in two-dimensional (2-D) photonic crystals (PhCs) deeply etched through monomode slab waveguides, e.g., AlGaAs/GaAs, GaAs/AlO_x, or InP/GaInAsP, suffer from radiation losses that are strongly affected by the air hole depth and shape. The issue of three-dimensional (3-D) out-of-plane losses is addressed analytically by means of an incoherent approximation. Assuming separability both for the dielectric map and for the electric field, this approach is valid for defects such as in-plane microcavities, PhC-based waveguides, bends and couplers. Out-of-plane scattering is translated into an effective imaginary index in the air holes, so that 3-D losses can be cast in a simple 2-D calculation. The case of cylindroconical holes is treated, and the validity of this approach is experimentally confirmed by transmission measurements through simple PhC slabs.

OCIS codes: 130.0130, 130.3130, 130.3060, 160.4760, 160.6000.

1. INTRODUCTION

In the past few years great effort has been devoted to the study of two-dimensional (2-D) photonic crystals (PhCs) at near-infrared wavelengths because of their potential to mold and guide light[1,2] and to lead to novel integrated optics (IO) applications.[3] Two different approaches have been exploited to characterize the performances and capabilities of 2-D PhC structures. The first consists of macroporous silicon-based systems almost infinite along the vertical direction.[4–8] This is, of course, a good model system, even though it requires collimated probe beams for optical measurements. On the other hand, the use of refractive-index confinement in the third dimension has favored the investigation of quasi-2-D PhCs.[9–13] In this second approach a 2-D PhC (e.g., a triangular lattice of air holes) is etched through a planar step-index waveguide. However, perforating the waveguide induces coupling of the guided wave to radiation modes into the claddings thus resulting in out-of-plane losses.[14–17] Only the case of perfect Bloch–Floquet modes with a sufficiently large wave vector below the light line of the claddings [i.e., the line $\omega = kc/n$ of the $\omega(k)$ dispersion diagram] allows lossless propagation.[17–19]

To keep out-of-plane scattering low, two approaches have been suggested. In the first approach high-index contrast slab waveguides are adopted, such as silicon-on-insulator systems[10,20,21] or thin (approximately half-wavelength) suspended membranes of high-index materials (e.g., GaAs, InP, and related alloys).[9,22,23] The use of a vertical monomode waveguide offers two advantages: it is a case of strong guiding, so that the requirement for etching is modest (i.e., 150–250 nm), or, in other words, the depth-to-diameter aspect ratio is of the order of unity. A different approach aims for conventional waveguides based on III–V materials grown on GaAs or InP substrates.[11–13,24–26] In this latter case, waveguiding is weak and etching is more difficult as one requires a depth such that the overlap of the guided-mode profile with the etched structure is as complete as possible.[11–16,24,27–29]

It has been demonstrated[17] that, in the case of high-contrast waveguides, absolutely lossless Bloch–Floquet modes well below the light line can propagate into a perfectly periodic PhC lattice. However, any practical use of light in optical devices, such as in-plane guides with bends or resonators, inevitably results in out-of-plane losses as it breaks the periodicity and the k conservation.

0740-3224/2003/030469-10$15.00

Thus, 2-D PhCs deeply etched in low-contrast slab guides have been demonstrated to be the preferable approach to reduce out-of-plane losses in compact PhC structures with many close-packed defects.[14,17] In this case, it has been pointed out that losses would be quite low if the PhC structure were sufficiently etched through the waveguide.[14,30] According to a scalar analytical perturbative approach,[14] losses scale as $(\Delta\varepsilon)^2$, i.e., the square of the dielectric constant step in the waveguide. For vanishing $\Delta\varepsilon$, the guided mode is unconfined and extends more into the claddings, approaching asymptotically the behavior of plane waves normal to arrays of infinitely deep holes. Therefore, no out-of-plane scattering is present provided that the etch depth can be increased along with the optical wave extension.

The possible application of PhC structures to IO devices has generated intense interest in the evaluation of out-of-plane losses in low-contrast systems. It has been shown[14–16] that the lowest-loss limit that can be expected in such structures corresponds to infinitely deep holes. In this ideal case, losses (referred to as intrinsic losses below) originate from two main sources. First is the modal mismatch between the confined mode that propagates in the bare waveguide and the Bloch mode that travels in the patterned region.[31] Second, the low-contrast waveguide approach implies that the PhC Bloch modes lie above the light line of the cladding layer and are intrinsically lossy.[18,19,32] In any case, even for this basic case the three-dimensional (3-D) problem is so complex that 3-D modeling of losses in PhC-based applications including several elements (e.g., guides, cavities, bends, etc.) is currently not possible. Therefore, a 2-D model that allows a significant reduction in computing efforts becomes a fundamental tool for the design of real devices.

In a previous paper[16] a 2-D model was used to investigate the role of the finite etch depth, and the results were confirmed by an exact 3-D numerical calculation. It was demonstrated that out-of-plane losses that are due to the hole depth scale such as $\Gamma(z)$, i.e., the fractional overlap of the guided mode with the unetched part of the holes. Moreover, the comparison of 3-D and 2-D loss calculations led to the validation of a phenomenological model for which out-of-plane scattering at the air holes is translated into effective dissipation.[14] Following this approach, losses are cast into a 2-D calculation by introducing a convenient loss parameter into the air holes (i.e., the imaginary coefficient ε'') that decreases with the hole depth, like $\Gamma(z)$.

Here, using the same scalar separability approach proposed by Benisty *et al.*,[14] we extend beyond the $\Gamma(z)$ scaling. First, we attempt to determine semianalytically the value of the loss parameter ε'' as a function of etch depth.[33] Second, we show that the same approach can be extended to treat any particular hole shape with oblique walls. In particular, we obtain an analytical expression for the frequent case of a cylindroconical hole shape in the cladding region of the waveguide. Finally, we assess the potential of our approach, present some experimental data, and analyze the data within the framework of the discussed ε'' loss model. We used an internal light source technique[11–13] to measure transmission spectra through simple PhC slabs for the TE polarization direction. The PhC structures consist of a triangular lattice of air holes deeply etched by electron–cyclotron resonance reactive ion etching through an InP/GaInAsP step-index waveguide. The experimental data are compared with 2-D finite-difference time-domain (FDTD) calculations that account for out-of-plane losses through a nonvanishing conductivity parameter $\sigma(\lambda) = (c/2\lambda)\varepsilon''$ introduced in the air holes.[34] On the other hand, the exact cylindroconical shape of the holes is determined from cross-sectional scanning electron microscopy (SEM) micrographs of PhC test structures etched in the same run as the measured PhC slabs.

In Section 2 we develop the separability approach for vertical wall holes that penetrate into the lower cladding: we show that our approach agrees with the results obtained from exact 3-D numerical models. In Section 3 we solve the case of cylindroconical holes and relate it to the previous case through a properly defined effective depth. In Section 4 we present and analyze the experimental data. Finally, we conclude by discussing the potential of our approach to provide a fundamental feedback to PhC fabrication. Although the SEM micrograph analysis gives only local information on the hole morphology, an average estimate is obtained from our model and predictions can be safely made on the fabrication improvements that are necessary to reduce losses.

2. HOLES WITH FINITE DEPTH AND VERTICAL WALLS

A typical quasi-2-D PhC structure etched through a conventional semiconductor step-index waveguide is sketched in Fig. 1. The vertical heterostructure is usually grown on a GaAs or InP substrate and consists of a bottom cladding (e.g., an Al-rich AlGaAs ternary compound or InP with refractive index n_1 and dielectric constant $\varepsilon_1 = n_1^2$), a core layer whose thickness is suited to monomode operation (e.g., GaAs or a lattice-matched GaInAsP alloy with refractive index n_2 and dielectric constant $\varepsilon_2 = n_2^2$), and a top cladding. The latter layer could be less confining than the bottom cladding: the confinement on the top side is ultimately enforced by the air. For simplicity we take the dielectric constant ε_1 also for the top cladding and, when necessary, we neglect the air, taking into consideration the system as vertically confined only by the symmetric dielectric profile $\varepsilon_1/\varepsilon_2/\varepsilon_1$. The holes are assumed to have the same shape (e.g., circular) with perfectly vertical walls and a flat bottom that penetrates into the lower cladding to a depth of z_0 [see

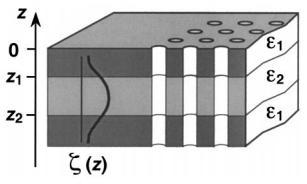

Fig. 1. Sketch of an ideal 2-D PhC etched through a conventional semiconductor step-index waveguide with a symmetric dielectric constant profile $\varepsilon_1/\varepsilon_2/\varepsilon_1$. The PhC consists of a triangular array of infinitely deep air holes. The top cladding thickness z_1, the core width (z_2-z_1), and the guided-mode profile $\zeta(z)$ are also shown.

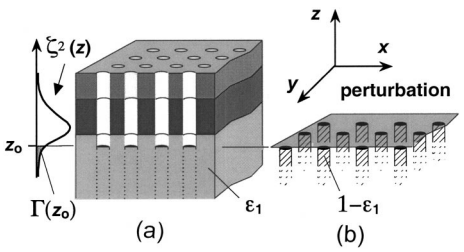

Fig. 2. (a) Same as Fig. 1 for the real case of a 2-D PhC with a finite hole depth z_0. The partial confinement factor $\Gamma(z_0)$ is also shown, i.e., the overlap integral of the squared field profile $\zeta^2(z)$ with the missing air column region [see Eq. (14)]; (b) sketch of the dielectric perturbation with respect to the case of infinitely deep holes.

Fig. 2(a)]. Here we do not consider the limiting situation of z_0 lying inside the core (i.e., $|z_0| < |z_2|$), which is well known to lead to important losses.

In the case of z_0 ranging in the bottom cladding (i.e., $|z_0| > |z_2|$), 3-D calculations[16] have led to the following first-order expression for the 2-D loss parameter:

$$\varepsilon'' = \varepsilon''_{\text{int}} + \varepsilon''_{\text{hole}}, \tag{1}$$

where $\varepsilon''_{\text{int}}$ accounts for intrinsic losses, whereas $\varepsilon''_{\text{hole}}$ contains contributions both from the finite etch depth and from the hole shape. The main sources of $\varepsilon''_{\text{int}}$ have been suggested in other papers[13–19,31,32] and were briefly commented on in Section 1. The $\varepsilon''_{\text{int}}$ values obtained from exact 3-D calculations for GaAs-based systems and the general scaling law deduced for ε'' by Benisty *et al.*[14] were used to extrapolate $\varepsilon''_{\text{int}}$ for the InP-based structures considered in Section 4. In any case, the analysis of theoretical and experimental results for both material systems[13,16] show that $\varepsilon''_{\text{int}}$ values are 1 order of magnitude lower than the actual ε'' values achievable with the current etching techniques. Therefore, at this stage $\varepsilon''_{\text{hole}}$ is the main factor that sets the loss level. Our aim in the following sections is to relate analytically this contribution to the hole shape parameters.

The real case of a 2-D PhC with finite hole depth is depicted in Fig. 2(a). The guided mode profile $\zeta(z)$ in the unetched waveguide is also shown. According to the separable approach, $\zeta(z)$ can also be assumed to be the mode profile in the PhC section. This is all the more true when PhC structures with modest air fill factor (f) values are considered (e.g., up to $f \sim 0.30$).[35]

We evaluated radiation losses induced by the finite hole depth by considering the actual PhC structure as the sum of the ideal system with infinitely deep holes (i.e., the intrinsic loss case) plus a dielectric perturbation. In our model the perturbation is represented by plugs of dielectric constant $\tilde{\varepsilon} = 1 - \varepsilon_1$ that extend from $z \to -\infty$ to z_0 [see Fig. 2(b)]. The choice of an infinite perturbation does not complicate the problem since the system is probed by waves of finite extent. For simplicity, the field of the ideal system at a given frequency ω is assumed to be scalar and its leaky character is neglected. By applying separability we can write the field as[14]

$$E(x, y, z) = \psi(x, y)\zeta(z). \tag{2}$$

Out-of-plane losses that are due to the finite hole depth are generated by the radiation of induced polarization

$$P(x, y, z) = E(x, y, z)\varepsilon_0\tilde{\varepsilon} = \psi(x, y)\zeta(z)\varepsilon_0\tilde{\varepsilon}, \tag{3}$$

with $|z| > |z_0|$. The dielectric plugs are infinite but, since perturbation $P(x, y, z)$ is taken only in the bottom cladding, it has the same exponential decay as $\zeta(z)$ toward the substrate [see Eq. (11)], i.e.,

$$P(x, y, z) \sim \exp(+Kz) \tag{4}$$

for $z \to -\infty$. Note that $K = 2\pi\,(n_{\text{eff}}^2 - n_1^2)^{1/2}/\lambda$ (where n_{eff} is the guided-mode effective index)[16] and $L_{\text{decay}} = 1/K$ can be considered as the effective height of the radiating volume. Equations (3) and (4) allow us to approximate the radiation of each plug as the radiation of an electric dipole p given by[14]

$$p = \iiint_{\text{plug volume}} P(x, y, z)\mathrm{d}x\mathrm{d}y\mathrm{d}z. \tag{5}$$

The useful vertical extension of dipole p is of the order of decay length L_{decay}. According to Benisty *et al.*,[16] it is possible to define to which extent the adopted approximation can be considered valid. In the Rayleigh–Gans approach[16] the field radiated by dielectric plug $\varepsilon(\mathbf{r})$ at location $\mathbf{r}'$ is given by the integral $I_{\text{RG}} = \iiint_V \times \varepsilon_0\varepsilon(\mathbf{r})E(\mathbf{r})\exp[i\mathbf{k}(\mathbf{r}' - \mathbf{r})]\mathrm{d}V$ (V is the radiating plug volume). Since $\varepsilon(\mathbf{r})$ is periodic, it can be expanded in a Fourier series in which the high-order components are weighted by a form factor that is a function of (D/a) with D and a equal to the hole diameter and the lattice period, respectively.[36] For modest fill factor values for which losses are low enough for device application,[35] this factor can be estimated to be 0.7–0.8 so that the contribution from high-order components in I_{RG} can be neglected. On the other hand, when the holes grow in size (i.e., f increases) the form factor decreases and the dipole approximation overestimates the radiation scattered by the perturbation. For example, when $f > 0.5$, i.e., $D > 0.75a$, the form factor reduces to a value lower than 0.5. Finally, in the investigated PhC structures $D < \lambda/2n_1$ and the integration on the hole surface in I_{RG} gives the hole section. The same argument applies in the z direction where the exponential decay of expression (4) has to be taken into account. Since even with refractive-index steps $\Delta n = n_2 - n_1 \sim 0.2$ typical of InP-based waveguides, $L_{\text{decay}} < \lambda/2n_1$, the approximation of Eq. (5) is reasonable, whereas it would break down in the case of weak waveguide confinement, i.e., $L_{\text{decay}} \geqslant \lambda/n_1$.

Different from the previous paper by Benisty *et al.*,[14] the dipole radiates in a homogeneous medium. The influence of the nearby waveguide compared with that of the cladding radiation modes is neglected. Hence, we can assume that all the power P_{rad} of the dipole radiation, i.e.,[37]

$$P_{\text{rad}} = \frac{p^2\omega^4 n_1}{12\pi\varepsilon_0 c^3} \tag{6}$$

is lost. Separating x, y, and z into Eq. (5) we obtain

$$P_{\text{rad}} = \frac{1}{2}\frac{\varepsilon_0\omega^4}{6\pi c^3} n_1\tilde{\varepsilon}^2\left[\iint_S \psi(x, y)\mathrm{d}x\mathrm{d}y\right]^2\left[\int_{-\infty}^{z_0}\zeta(z)\mathrm{d}z\right]^2. \tag{7}$$

For comparison, let us look at the power lost by dissipation in a system in which the air holes have a fictitious dissipative nature represented by an imaginary dielectric constant $\varepsilon''_{\text{hole}}$. The latter constant is assumed to be homogeneous over the z axis to enable a simple 2-D calculation. The dissipated power can be written as

$$P_{\text{diss}} = \frac{1}{2}\varepsilon_0\omega\varepsilon''_{\text{hole}}\int\int\int_{\text{holes}} E^2(x, y, z)\,\mathrm{d}x\,\mathrm{d}y\,\mathrm{d}z = \frac{1}{2}\varepsilon_0\omega\varepsilon''_{\text{hole}}\int\int_S \psi^2(x, y)\,\mathrm{d}x\,\mathrm{d}y\int_{-\infty}^{+\infty}\zeta^2(z)\,\mathrm{d}z, \quad (8)$$

where S denotes the hole cross section of area S_{hole} and the integral on $\zeta(z)$ runs over the whole z axis. Note that the field is squared before the integral is taken and coherence effects are neglected. This can be justified if we observe that (i) the dissipation acts in a local manner, (ii) the dipoles sit close to the hole bottom[16] thus emitting in a 3-D medium (i.e., the bottom cladding) far from the structured top dielectric region, (iii) disorder in real PhC structures introduces spatial incoherence. Moreover, assuming that the field $\psi(x, y)$ has no strong variations inside a hole, we make the following approximation:

$$\left[\int\int_S \psi(x, y)\,\mathrm{d}x\,\mathrm{d}y\right]^2 \approx S_{\text{hole}} \times \int\int_S \psi^2(x, y)\,\mathrm{d}x\,\mathrm{d}y. \quad (9)$$

Then, comparing Eqs. (7) and (8) leads to the general expression for $\varepsilon''_{\text{hole}}$:

$$\varepsilon''_{\text{hole}} = \tilde{\varepsilon}^2\frac{1}{6\pi c^3}\omega^3 n_1\frac{\left[\int_{-\infty}^{z_0}\zeta(z)\,\mathrm{d}z\right]^2}{\int_{-\infty}^{+\infty}\zeta^2(z)\,\mathrm{d}z}S_{\text{hole}}. \quad (10)$$

Taking into account the exponential decay of $\zeta(z)$ in the bottom cladding ($z \to -\infty$),

$$\zeta(z) = A\exp(+Kz), \quad (11)$$

we find that

$$\left[\int_{-\infty}^{z_0}\zeta(z)\,\mathrm{d}z\right]^2 = \frac{2}{K}\int_{-\infty}^{z_0}\zeta^2(z)\,\mathrm{d}z\,. \quad (12)$$

Finally, substituting Eq. (12) into Eq. (10) and replacing ω/c by $2\pi/\lambda$ yields

$$\varepsilon''_{\text{hole}} = \tilde{\varepsilon}^2\frac{8\pi^2}{3\lambda^3}n_1\Gamma(z_0)L_{\text{decay}}S_{\text{hole}}, \quad (13)$$

where

$$\Gamma(z_0) = \frac{\int_{-\infty}^{z_0}\zeta^2(z)\,\mathrm{d}z}{\int_{-\infty}^{+\infty}\zeta^2(z)\,\mathrm{d}z} \quad (14)$$

is the partial confinement factor,[16] i.e., the overlap integral of the squared field profile $\zeta^2(z)$ with the missing air column region.

Equation (13) indicates that (i) the size of the radiating volume is $L_{\text{decay}}S_{\text{hole}}$ instead of $V = w\,S_{\text{hole}}$ (where w is the core width) as in the equivalent formula by Benisty *et al.*,[14] (ii) the loss parameter $\varepsilon''_{\text{hole}}$ scales like $\Gamma(z_0)$, as already pointed out in previous papers.[15,16] The new feature of Eq. (13) is that it provides a quantitative value for coefficient B in the relation $\varepsilon''_{\text{hole}} = B\Gamma(z_0)$.[16] Let us examine the case of a GaAs-based PhC structure already illustrated elsewhere.[14–16] Taking $\lambda = 0.98\,\mu$m, $\varepsilon_1 = 9.4$, $\tilde{\varepsilon}^2 \sim 70$, and $K \sim 10$ [i.e., $L_{\text{decay}} = 100$ nm, thus justifying the assumption of Eq. (5)] for $f = 0.25 \pm 0.05$ and for a triangular lattice period $a = 240$–260 nm, we find $B/f = 35$, in good agreement with the value $B/f \approx 30$ obtained by exact 3-D calculations.[15,16] The adopted air fill factor range accounts for both fluctuations in the PhC fabrication and discrepancies between 2-D and 3-D calculated f values.[38] The last result clearly proves the potentials of this approach to orient the design of low-loss PhC systems. With Eq. (13) it is possible to determine how any figure of merit (e.g., losses in a simple crystal or in a one-dimensional Fabry–Perot cavity) is influenced by etching parameters.

Equation (13) is plotted in Fig. 3 for three basic material systems for IO applications: (a) refers to a typical GaAs/AlO_x-based 2-D PhC ($\lambda = 1.5\,\mu$m, $n_1 = 1.61$, $n_2 = 3.37$, and $a \sim 400$ nm)[39]; (b) is for an $Al_xGa_{1-x}As$/GaAs structure with $x = 0.80$ in the bottom cladding ($\lambda = 1.0\,\mu$m, $n_1 = 3.0$, $n_2 = 3.5$, and $a \sim 240$–260 nm);[11,12,16] and (c) represents the case of an InP/GaInAsP system ($\lambda = 1.5\,\mu$m, $n_1 = 3.17$, $n_2 = 3.35$, and $a \sim 400$ nm; see also Section 4).[13] According to our assumptions, the three curves are shown only for z_0 values lying in the bottom cladding (i.e., $|z_0| > |z_2|$). When $f = 0.30$ we obtain $B \sim 0.2$, 10, and 20 for (a), (b), and (c), respectively. Apart from the scaling constant B, the dependence of $\varepsilon''_{\text{hole}}$ on etching depth $|z_0|$ is given by the fun-

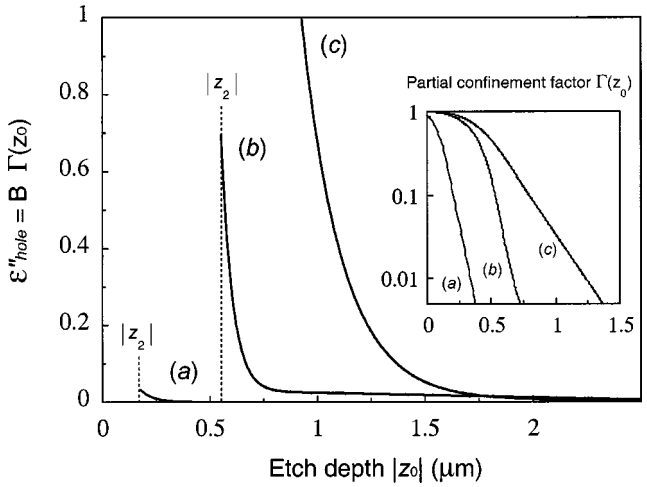

Fig. 3. Estimate of the loss parameter $\varepsilon''_{\text{hole}} = B\Gamma(z_0)$ as a function of the etched depth $|z_0|$ for hole diameters that correspond to typical air-fill factor values of $f = 0.20$–0.30. Three basic material systems are considered: (a) a typical GaAs/AlO_x-based 2-D PhC, (b) an $Al_xGa_{1-x}As$/GaAs structure, (c) an InP/GaInAsP system. The curves are shown only for z_0 values lying in the bottom cladding (i.e., $|z_0| > |z_2|$; see Figs. 1 and 2). The partial confinement factor $\Gamma(z_0)$ is plotted in the inset for the three cases.

damental quantity $\Gamma(z_0)$, which is shown in the inset of Fig. 3 on a semilogarithmic plot. Three parameters contribute to shape $\Gamma(z_0)$: (i) the refractive-index step of the waveguide, (ii) the core thickness, and (iii) to a lesser extent, the top cladding thickness. Since $K \propto n_{\text{eff}}$, the slope of the curves illustrated in Fig. 3 is determined by n_{eff}. Then, for a given K, the waveguide parameters [i.e., (i)–(iii)] set the value of factor A in Eq. (11). Once z_0 is fixed, it is thus possible for one to minimize $\Gamma(z_0)$ (i.e., $\varepsilon''_{\text{hole}}$) by varying the heterostructure parameters (e.g., the three-alloy compositions, the core and top cladding thickness). Nevertheless, because of the importance of achievable depth z_0, this minimization cannot be usefully performed before a thorough investigation of the etching performances as a function of material properties (e.g., the alloy composition) has been well established.

3. HOLES WITH OBLIQUE WALLS: ANALYTICAL FORMULA FOR CYLINDROCONICAL HOLES

Unfortunately, the picture of straight holes with a flat bottom is not realistic in most practical cases. In general, vertical sidewalls can be achieved only in the top part of etched holes, whereas oblique walls tend to occur at the bottom. Such deviations from the vertical could be due to overetching or underetching. Here we present a study of the underetching case, even though the same approach can be, in principle, adapted to other shapes. In particular we will be able to obtain an analytical expression for $\varepsilon''_{\text{hole}}$ for cylindroconical holes. For simplicity, we restrict this analytical approach to holes that are perfectly cylindrical in the top cladding and in the core, while their conical portion is located entirely inside the bottom cladding (see Fig. 4). To exploit the results discussed in Section 2 we define the quantity z_{eq} as the equivalent depth of an ideal cylindrical hole that gives the same amount of loss as the actual cylindroconical hole. Then, it would be possible for us to determine $\varepsilon''_{\text{hole}}$ by introducing the calculated z_{eq} value in Eq. (13) (i.e., taking $z_0 = z_{\text{eq}}$).

The assumed cylindroconical hole shape is sketched in Fig. 4. The cone apex lies at z_a, whereas its base is located at $z_b = z_a + \Delta z$, where the cylindrical part ends. If Δz is the cone height and α is the cone half-angle, the hole radius r is given by $r = \Delta z \tan\alpha$. We note that in real cases variations of cone slope α can occur along the z axis [see, for example, Fig. 6(b)]. Nevertheless, since the system is probed by a guided beam with an exponentially decaying profile $\zeta(z)$ in the bottom cladding, a perfect conical shape can be assumed if slope α remains constant for some L_{decay} terms (see Section 4).

The shape of perturbation $\tilde{\varepsilon}(x, y, z)$ is now complementary to the air cone. As in Eq. (5), we can cast the perturbation of each hole in a single radiating dipole p. Again, we can assume that $\psi(x, y)$ is constant at the length scale of interest. To take into account the effect of the different hole shape it is sufficient to replace

$$\int_{-\infty}^{z_0} \zeta(z)\mathrm{d}z \rightarrow \int_{-\infty}^{z_b} g(z)\zeta(z)\mathrm{d}z, \tag{15}$$

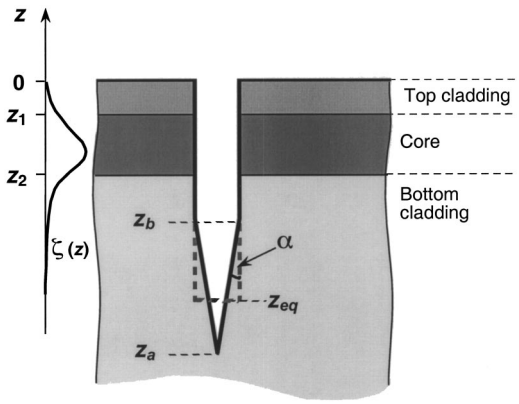

Fig. 4. Sketch of the cylindroconical hole shape model. The main geometric parameters and the guided field profile $\zeta(z)$ are shown. z_{eq} is defined as the equivalent depth of a cylindrical hole that gives the same amount of losses as the tapered-bottom hole.

where the factor $g(z)$ accounts for the fractional amount of material left as a perturbation at depth z. Expression (15) is quite general and, if we choose the right function $g(z)$, it can be used to treat different hole shapes. Moreover, $g(z)$ can be either positive (as in the present case) or negative (i.e., the missing material case).

For the cylindroconical hole shape depicted in Fig. 4, $g(z)$ takes the following form:

$$\begin{aligned} g(z) &= 1 && (|z| > |z_a|), \\ g(z) &= 1 - \frac{r(z)^2}{r^2} && (|z_b| < |z| < |z_a|), \end{aligned} \tag{16}$$

where $r(z) = \tan\alpha(z - z_a)$ is the local cone radius. Then, the right-hand integral in expression (15) splits into two parts:

$$\begin{aligned} \int_{-\infty}^{z_b} g(z)\zeta(z)\mathrm{d}z = & \int_{-\infty}^{z_a} \exp[-K(z - z_a)]\mathrm{d}z \\ & + \int_{z_a}^{z_b}\left[1 - \frac{r(z)^2}{r^2}\right] \\ & \times \exp[-K(z - z_a)]\mathrm{d}z. \end{aligned} \tag{17}$$

In Eq. (17) we have omitted the normalization factor A of Eq. (11) and have taken z_a as the local origin, thus writing the field profile as $\zeta(z) = \exp[-K(z - z_a)]$. From Eq. (17) we obtained the following result:

$$\begin{aligned} \int_{-\infty}^{z_b} g(z)\zeta(z)\mathrm{d}z = & \frac{2}{K}\exp(K\Delta z)\left[\frac{1}{K\Delta z}\right. \\ & \left. - \frac{1 - \exp(-K\Delta z)}{K^2\Delta z^2}\right]. \end{aligned} \tag{18}$$

In principle, the next step could be to inject Eq. (18) into Eq. (10) to achieve an analytical formula for $\varepsilon''_{\text{hole}}$. However, it is more instructive to attempt a comparison between the ideal flat bottom case and the real conical bottom case. To this extent we introduce the equivalent depth z_{eq}, which represents the depth of a cylindrical hole

giving the same radiating dipole as a cylindroconical hole. In this case $g(z) = 1$ from $-\infty$ to z_{eq} and the right-hand integral of expression (15) can be written as

$$\int_{-\infty}^{z_{eq}} \zeta(z)\mathrm{d}z = \frac{1}{K}\exp[K(z_{eq} - z_b)] = \frac{1}{K}\exp(K\Delta z)\exp[K(z_{eq} - z_b)]. \quad (19)$$

Following the definition of z_{eq}, we can equate the right-hand sides of Eqs. (18) and (19), thus obtaining

$$\exp[-K(z_b - z_{eq})] = 2\left[\frac{1}{K\Delta z} - \frac{1 - \exp(-K\Delta z)}{K^2\Delta z^2}\right]. \quad (20)$$

This simple formula expresses z_{eq} as an analytical function of K and, implicitly, of the cone angle $\alpha = \tan^{-1}(r/\Delta z)$. Since Eq. (20) allows one to take into account different hole shapes and to compare their losses, it can be seen as a useful tool for optimization of the etching techniques that are used for the fabrication of PhC structures.

Finally, two asymptotic cases can be identified for Eq. (20): (i) $K\,\Delta z \to 0$, i.e., the flat bottom limit; and (ii) $K\,\Delta z \to \infty$, i.e., the vertical wall limit. By examining their physical interpretation, one can easily determine that L_{decay} sets the crossover between the two regimes (see Fig. 5).

When $K\,\Delta z \to 0$ [see Fig. 5(a)], the decay of $\zeta(z)$ is slow compared with the cone height and the perturbation can be expected to be volume averaged. By developing the exponential factors, the right-hand side of Eq. (20) can be written as $(1 - K\,\Delta z/3)$, so that

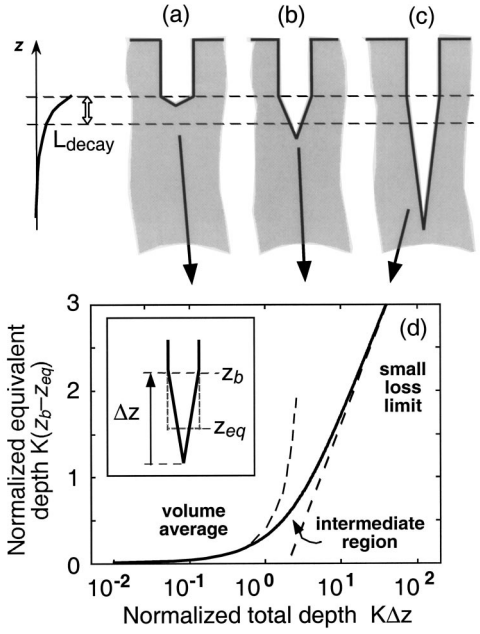

Fig. 5. Illustration of three different cases for losses with cylindroconical holes: (a) cone height Δz much smaller than the decay length $L_{decay} \sim 1/K$ of the guided mode: flat bottom limit; (b) intermediate case: $\Delta z \sim L_{decay}$; (c) $\Delta z \gg L_{decay}$: vertical wall limit; (d) plot of the normalized equivalent depth $K(z_b - z_{eq})$ as a function of the normalized total depth $K\Delta z$.

$$z_b - z_{eq} = \frac{\Delta z}{3}, \quad (21)$$

which is exactly equivalent to a volume average.

In contrast, in the $K\,\Delta z \to \infty$ regime, the decay of $\zeta(z)$ is much faster than the hole narrowing [see Fig. 5(c)]. In this limit losses are supposed to be low and Eq. (20) gives

$$z_b - z_{eq} = -\frac{1}{K}\ln\left(\frac{2}{K\ \Delta z}\right), \quad (22)$$

which means that the equivalent flat bottom is situated at many decay lengths from the base of the cone at z_b. The evolution of z_{eq} is logarithmic with Δz, but, according to Eqs. (10) and (19), ε''_{hole} depends on the squared dipole term $[\int_{-\infty}^{z_{eq}} \zeta(z)\mathrm{d}z]^2 \propto \exp[-2K(z_b - z_{eq})]$, which scales like Δz^{-2} [see Eq. (22)]. From this result we can conclude that in the vertical hole limit the main contribution for losses comes from the top region of the cone, within a few decay lengths from z_b. In this region the amount of extra material (leading to a radiating polarization) scales like $L_{decay}/\Delta z$ as the exponential factor $\exp[-K(z_b - z_{eq})]$. In practical cases it is difficult to achieve holes with a well-defined conical shape and high Δz values. Moreover, when Δz is high the irregularities of the hole shape, including the core region, are likely to play an important role. Losses are then more difficult to quantify systematically, but one can hope that their level becomes sufficiently low for high-performance applications, such as filters with high quality factors, low-loss waveguides, and bends.

Finally, in the intermediate regime $K\,\Delta z \sim 1$ [see Fig. 5(b)] no simple explanation holds. The dimensionless version of Eq. (20) is plotted in Fig. 5(d), where the two asymptotic regimes are illustrated as dashed lines.

4. COMPARISON WITH EXPERIMENTAL DATA

The analytical model described in Sections 3 and 4 has been developed for PhC structures with imperfect holes both in depth and shape. Because of the assumptions made, the above approach fails when perfect infinitely deep holes are considered. This intrinsic loss limit (see Section 2) has been preliminarily tackled in a 2-D first-order approximation[14] and has been discussed within the framework of a 3-D model yielding the value $\varepsilon''_{int} = 0.02–0.04$ for 2-D PhCs etched through AlGaAs/GaAs waveguides.[15,16] We point out that (i) different 2-D models[17] validate the basic scaling rule[13,14]

$$\varepsilon''_{int} \propto \frac{w}{\lambda/n_2}(u^2 f)(\Delta\varepsilon)^2\eta\Gamma_2, \quad (23)$$

where $\Delta\varepsilon = \varepsilon_2 - \varepsilon_1$, w is the core thickness, $u = a/\lambda$ is the dimensionless reduced frequency, η is the extraction efficiency for a dipole in the core, and $\Gamma_2 = \int_{core}|\zeta(z)|^2\mathrm{d}z/\int|\zeta(z)|^2\mathrm{d}z$ is the confinement factor in the core. (ii) The 3-D calculated ε''_{int} values can be taken as reference. (iii) The overall losses are additive, i.e., $\varepsilon'' = \varepsilon''_{int} + \varepsilon''_{hole}$ [see Section 2, Eq. (1)]. The weak mode confinement in the InP/GaInAsP waveguide considered in this section leads to ε''_{int} values lower than those reported

above for the AlGaAs/GaAs systems. In particular, assuming the structure parameters listed below and the scaling of Eq. (23), $\varepsilon''_{\text{int}} \sim 0.01-0.02$ is obtained. Then our analysis can concentrate on the hole shape contribution $\varepsilon''_{\text{hole}}$, for which optical measurements can yield a fundamental feedback to PhC fabrication.

The 2-D PhCs that consist of a triangular lattice of air holes were fabricated on nominally undoped GaInAsP/InP heterostructures grown on *n*-InP substrates [see Fig. 6(a)].[13] Moderate fill factor values ($f \sim 0.30$) were chosen to minimize the out-of-plane scattering.[11–13] Such low *f* values result in a full gap only for TE polarization. The PhC structures were etched vertically through an InP/GaInAsP/InP slab waveguide with a 434-nm-thick $Ga_{0.24}In_{0.76}As_{0.52}P_{0.48}$ core ($n_2 = 3.35$) sandwiched between a 200-nm-thick InP cap layer and a 600-nm-thick InP buffer layer ($n_1 = 3.17$). In the spectral region of interest (i.e., $\lambda \sim 1.55\ \mu$m), the waveguide can be regarded as monomode and the fundamental TE mode has an effective index of $n_{\text{eff}} = 3.24$.[13] An internal light source was embedded in the core layer. It consists of two different GaInAsP strain-compensated quantum well packages that emit at 1.47 and 1.55 μm, respectively, which are separated by a 30-nm spacer and located approximately in the middle of the guiding structure between two 181-nm-thick barrier layers. The superimposition of the two quantum well signals yields a 100-nm-wide photoluminescence peak centered at 1500 nm.[13]

Electron-beam (e-beam) lithography was used to define the PhC patterns that were transferred to the semiconductor heterostructure by electron–cyclotron resonance reactive ion etching.[13,40] A cross-sectional view SEM micrograph of the PhCs obtained is illustrated in Fig. 6(b). The hole shape is cylindroconical with an elongated tapered bottom and nearly vertical walls close to the surface. Some fluctuations appear in the hole depth around the average value $\langle |z_a| \rangle \geqslant 3\ \mu$m, whereas no bending is present and the holes have straight walls down to $|z_2| = 634$ nm. As shown in the inset of Fig. 6(b), any tilting

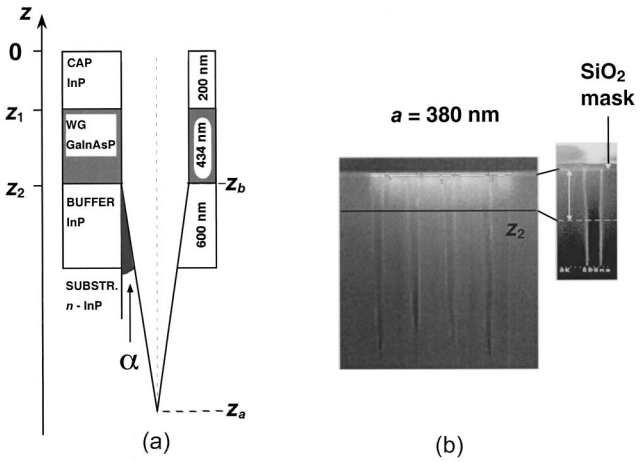

Fig. 6. (a) Sketch of the InP/GaInAsP waveguide (WG) heterostructure. The cylindroconical hole shape deduced from the SEM analysis of the sample is illustrated. (b) Edge view SEM micrograph of a test PhC structure for the studied sample. The image was taken before the removal of the SiO_2 mask. In the inset the almost cylindrical shape of the holes down to z_2 is evident.

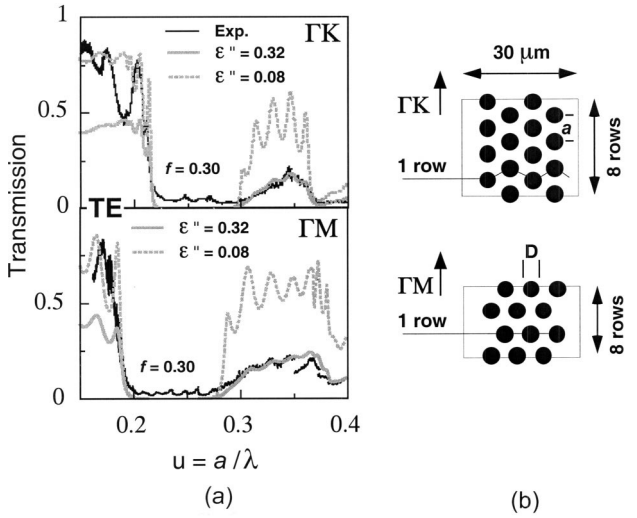

Fig. 7. (a) TE transmission spectra through Γ*M* and Γ*K* oriented PhC slabs for the sample in Fig. 6. Experimental spectra (boldface curves) are compared with 2-D FDTD calculated spectra (lightface curves). (b) Sketch of the typical layout of simple PhC structures along Γ*M* and Γ*K* orientations. Each slab is eight rows thick and is characterized by the period *a* (or hole diameter *D*) value. Hairlines show a single atomic plane for both orientations.

of the sidewalls in the core ($|z| < |z_2|$) is negligible, whereas the conical part lies completely inside the lower cladding ($|z| > |z_2|$). Therefore, the hole shape model sketched in Fig. 6(a) can be assumed.

An internal light source technique[11–13] was used to measure transmission spectra through PhC slabs. The photoluminescence excited inside the quantum wells was used as a built-in probe beam. Part of the photoluminescence signal propagates parallel to the surface as a guided mode and interacts with the PhC structure before it escapes from a cleaved edge at which adequate light collection is performed.[11–13] The absolute PhC transmission is obtained by normalizing the spectrum measured after transmission through the PhC slab with respect to a spectrum collected in a nonpatterned region of the sample. Details of the experimental setup are given elsewhere.[13] Here, we note that, since internal light source measurements on a single PhC structure yield the transmission spectrum only in a narrow interval (~100 nm), the lithographic tuning approach was used and PhC structures with different periods *a* were measured ($a = 240-640$ nm; $\Delta a = 20$ nm). If *f* is kept constant, the scaling property of PhCs[1] allows one to explore the whole photonic bandgap by plotting all the spectra as a function of dimensionless frequency *u*.[11–13]

Transmission spectra through eight-rows-thick PhCs along both Γ*M* and Γ*K* orientations and for TE polarization are shown in Fig. 7(a). The layout of simple PhC slabs is sketched in Fig. 7(b). Well-defined PBGs appear in each spectrum with steep dielectric band edges at $u = 0.19$ and 0.22 for Γ*M* and Γ*K* orientations, respectively. On the other hand, because of the strong influence of out-of-plane losses at the air band edge,[12] smooth transmission bands appear at $u \approx 0.28$ and 0.30 for Γ*M* and Γ*K*, respectively. Transmission values between 80% and 90% are reached for $u < 0.20$, whereas they are less

than 40% for $u > 0.30$. Finally, an average transmission of $T \sim 3-5\%$ is observed inside the PBG.

The experimental spectra are compared with theoretical spectra calculated with a 2-D FDTD model.[34,41–44] The vertical confinement in the waveguide was taken into account assuming that $n \equiv n_{\mathrm{eff}} = 3.24$ for the dielectric matrix. Out-of-plane losses were cast into the 2-D calculation by introducing the phenomenological loss parameter into the air holes (i.e., the conductivity $\sigma = (c/2\lambda)\varepsilon''$, see Section 1).[34] The air fill factor f and ε'' were chosen as the only free parameters of the fit.[45] The fitted curves are shown in Fig. 7(a). Experimental and calculated spectra are in good agreement for both orientations. We note that different ε'' values have to be used to fit either the dielectric or the air band. This discrepancy is due to the general scaling rule reported in Eq. (23) (i.e., $\varepsilon'' \propto u^2 f$): if f is constant, while decreasing u, lower ε'' values have to be introduced to fit the transmission spectra. However, the following analysis will concentrate only on the air band, which is intrinsically the most sensitive to out-of-plane scattering in the air holes.[1]

From the fit of the air transmission band, the total loss parameter value $\varepsilon'' = 0.32 \pm 0.020$ is obtained [see Fig. 7(a)]. Then, the analytical approach of Section 3 can be applied to determine the different contributions to out-of-plane losses. Since $\varepsilon''_{\mathrm{int}} \sim 0.01-0.02$ (see above), Eq. (1) gives the shape factor value $\varepsilon''_{\mathrm{hole}} = 0.305 \pm 0.025$. On the other hand, from the SEM micrograph analysis the cone slope α in the first L_{decay} can be determined. From Fig. 6(b), taking into account that $L_{\mathrm{decay}} \sim 360$ nm, the value $\alpha \sim 2.5° \pm 0.5°$ is deduced. Moreover, Fig. 6(b) shows clearly that in actual PhC structures holes are not perfectly conical and α varies along z. Nevertheless, because of the exponential decay of the perturbation, losses depend mostly on the hole shape in the first decay length. As illustrated in Section 3, when K is fixed $\varepsilon''_{\mathrm{hole}}$ is a function of α, provided that the cone slope remains constant at least down to z_{eq}. Once the shape model of Fig. 6(a) is assumed (i.e., $z_b = z_2$ in Fig. 4), Eqs. (20) and (13) (with $z_0 = z_{\mathrm{eq}}$) yield the calculated value $\varepsilon''_{\mathrm{hole}} = 0.30$, which is in perfect agreement with the experimental data. Therefore, an important conclusion can be drawn for real cylindroconical PhC structures: in a first-order approximation, the contribution $\varepsilon''_{\mathrm{hole}}$ does not depend on the cone height (i.e., the effective etch depth) but on angle α, which can be identified as the basic hole shape parameter to assess out-of-plane losses quantitatively.

Extrapolating from this analysis, two perspectives emerge for the fabrication of low-loss PhC structures. First, it is found that the minimum loss limit $\varepsilon''_{\mathrm{int}}$ could be reached for $\alpha < 0.5°$, i.e., for holes with almost straight walls in some L_{decay} terms inside the substrate. On the other hand, a loss level sufficiently low for good performance IO applications (e.g., $\varepsilon'' \leqslant 0.1$)[16] could be achieved for $\alpha < 1.5°$, a reduction in the cone slope that might already be feasible with the current etching techniques.

5. CONCLUSION

We have presented an electromagnetic analysis of radiation losses induced in planar PhCs etched through conventional waveguides by insufficient hole depth and cylindroconical hole shape. The separability of the 3-D dielectric constant map has been assumed. A phenomenological approach has been adopted to model losses in the 2-D projection of the PhC system. In particular, an imaginary dielectric constant has been added to the air holes to account for out-of-plane scattering. The latter constant has been decomposed into an intrinsic loss term ($\varepsilon''_{\mathrm{int}}$) and a hole shape factor ($\varepsilon''_{\mathrm{hole}}$). The problems of cylindrical holes of finite depth and of conical holes in the bottom cladding have been analytically solved. In the second case, simple formulas allow for good physical insight into the various loss regimes that depend on the relative values of the cone depth and of the guided-mode decay length.

This model has proved to be a powerful tool that avoids the task of heavy 3-D calculations in the design of many PhC applications. From a more general point of view, the underlying assumption of incoherent scatterers[14] presents further advantages for the modeling of complex PhC-based devices: it is independent of the particular architecture being considered.

To validate this analysis, the case of a 2-D triangular PhC etched through an InP-based waveguide has been considered. PhC slabs were fabricated by electron–cyclotron resonance reactive ion etching to obtain cylindroconical holes with a conical bottom in the lower cladding. Transmission measurements were performed by use of an internal probe technique. Experimental data were compared to 2-D FDTD calculated spectra and a total loss value of $\varepsilon'' = 0.32$ was obtained. This value is in good agreement with the model prediction if cone angle α in the first L_{decay} in the bottom cladding is taken as the hole shape parameter. This is justified by the assumption of an exponential decaying perturbation, provided that no strong variations of α occur in some decay lengths.

The combination of theoretical and experimental results has led to a through investigation of the hole shape contributions to out-of-plane losses. In the real case of cylindroconical holes, the cone angle α has been clearly identified as a fundamental parameter to assess quantitatively the PhC quality and the performances of PhC-based devices.

Finally, the presented analysis is a useful tool to provide efficient feedback for detailed fabrication parameters in terms of fine optical properties of the PhC structures. The quantitative estimate of out-of-plane losses is an important step toward the design and fabrication of low-loss PhC-based IO devices. Clear perspectives can be identified for the fabrication process, whereas optical measurements can be used to check and to validate the progress of etching techniques.

ACKNOWLEDGMENTS

The authors acknowledge S. Anand from the Royal Institute of Technology, Kista, Sweden, for the InP/GaInAsP heterostructure growth. This research was supported by the European Union within the framework of the Information Society Technologies (IST) project Photonic Crystals Integrated Circuits (PhCIC), contract 1999–11239.

R. Ferrini's e-mail address is rolando.ferrini @epfl.ch.

REFERENCES AND NOTES

1. J. D. Joannopoulos, R. D. Meade, and J. N. Winn, *Molding the Flow of Light* (Princeton University, Princeton, N.J., 1995).
2. H. Benisty, S. Olivier, M. Rattier, and C. Weisbuch, "Applications of two-dimensional photonic crystals to semiconductor optoelectronics devices," in *Photonic Crystals and Light Localization in the 21st Century*, C. M. Soukoulis, ed. (Kluwer Academic, Dordrecht, The Netherlands, 2001), pp. 117–127.
3. A. Sharkawy, S. Shi, and D. Prather, "Multichannel wavelength division multiplexing with photonic crystals," Appl. Opt. **40**, 2247–2252 (2001).
4. U. Gruning, V. Lehmann, S. Ottow, and K. Busch, "Macroporous silicon with a complete two-dimensional photonic band gap centered at 5 μm," Appl. Phys. Lett. **68**, 747–749 (1996).
5. S. W. Leonard, H. M. van Driel, K. Busch, S. John, A. Birner, A. P. Li, F. Muller, U. Gosele, and V. Lehmann, "Attenuation of optical transmission within the band gap of thin two-dimensional macroporous silicon photonic crystals," Appl. Phys. Lett. **75**, 3063–3065 (1999).
6. S. Rowson, A. Chelnokov, and J. M. Lourtioz, "Two-dimensional photonic crystals in macroporous silicon: from mid-infrared (10 μm) to telecommunication wavelengths (1.3–1.5 μm)," J. Lightwave Technol. **17**, 1989–1995 (1999).
7. R. B. Wehrspohn, A. Birner, J. Schilling, F. Mueller, R. Hillebrand, and U. Gösele, "Photonic crystals from macroporous silicon," in *Photonic Crystals and Light Localization in the 21st Century*, C. M. Soukoulis, ed. (Kluwer Academic, Dordrecht, The Netherlands, 2001), pp. 143–153.
8. J. Schilling, R. B. Wehrspohn, A. Birner, F. Muller, R. Hillebrand, U. Gosele, S. W. Leonard, J. P. Mondia, F. Genereux, H. M. van Driel, P. Kramper, V. Sandoghdar, and K. Busch, "A model system for two-dimensional and three-dimensional photonic crystals: macroporous silicon," J. Opt. A. Pure Appl. Opt. **3**, S121–S132 (2001).
9. A. Scherer, O. Painter, B. D'Urso, R. Lee, and A. Yariv, "InGaAsP photonic band gap crystal membrane microresonators," J. Vac. Sci. Technol. B **16**, 3906–3910 (1998).
10. S. Y. Lin, E. Chow, S. G. Johnson, and J. D. Joannopoulos, "Demonstration of highly efficient waveguiding in a photonic crystal slab at the 1.5-μm wavelength," Opt. Lett. **25**, 1297–1299 (2000).
11. D. Labilloy, H. Benisty, C. Weisbuch, T. F. Krauss, R. Houdré, and U. Oesterle, "Use of guided spontaneous emission of a semiconductor to probe the optical properties of two-dimensional photonic crystals," Appl. Phys. Lett. **71**, 738–740 (1997).
12. H. Benisty, C. Weisbuch, D. Labilloy, M. Rattier, C. J. M. Smith, T. F. Krauss, R. M. De la Rue, R. Houdré, U. Oesterle, C. Jouanin, and D. Cassagne, "Optical and confinement properties of two-dimensional photonic crystals," J. Lightwave Technol. **17**, 2063–2077 (1999).
13. R. Ferrini, D. Leuenberger, M. Mulot, M. Qiu, J. Moosburger, M. Kamp, A. Forchel, S. Anand, and R. Houdré, "Optical study of two-dimensional InP-based photonic crystals by internal light source technique," IEEE J. Quantum Electron. **38**, 786–799 (2002).
14. H. Benisty, D. Labilloy, C. Weisbuch, C. J. M. Smith, T. F. Krauss, D. Cassagne, A. Beraud, and C. Jouanin, "Radiation losses of waveguide-based two-dimensional photonic crystals: positive role of the substrate," Appl. Phys. Lett. **76**, 532–534 (2000).
15. P. Lalanne and H. Benisty, "Out-of-plane losses of two-dimensional photonic crystals waveguides: electromagnetic analysis," J. Appl. Phys. **89**, 1512–1514 (2001).
16. H. Benisty, P. Lalanne, S. Olivier, M. Rattier, C. Weisbuch, C. J. M. Smith, T. F. Krauss, C. Jouanin, and D. Cassagne, "Finite-depth and intrinsic losses in vertically etched two-dimensional photonic crystals," Opt. Quantum Electron. **34**, 205–215 (2002).
17. W. Bogaerts, P. Bienstman, D. Taillaert, R. Baets, and D. De Zutter, "Out-of-plane scattering in photonic crystal slabs," IEEE Photonics Technol. Lett. **13**, 565–567 (2001).
18. S. G. Johnson, S. H. Fan, P. R. Villeneuve, J. D. Joannopoulos, and L. A. Kolodziejski, "Guided modes in photonic crystal slabs," Phys. Rev. B **60**, 5751–5758 (1999).
19. E. Chow, S. Y. Lin, S. G. Johnson, P. R. Villeneuve, J. D. Joannopoulos, J. R. Wendt, G. A. Vawter, W. Zubrzycki, H. Hou, and A. Alleman, "Three-dimensional control of light in a two-dimensional photonic crystal slab," Nature **407**, 983–986 (2000).
20. N. Fukaya, D. Ohsaki, and T. Baba, "Two-dimensional photonic crystal waveguides with 60 degrees bends in a thin slab structure," Jpn. J. Appl. Phys. **39**, 2619–2623 (2000).
21. A. Shinya, M. Notomi, I. Yokohama, C. Takahashi, J. I. Takahashi, and T. Tamamura, "Two-dimensional Si photonic crystals on oxide using SOI substrate," Opt. Quantum Electron. **34**, 113–121 (2002).
22. X. Letartre, C. Seassal, C. Grillet, P. Rojo-Romeo, P. Viktorovitch, M. L. d'Yerville, D. Cassagne, and C. Jouanin, "Group velocity and propagation losses measurement in a single-line photonic-crystal waveguide on InP membranes," Appl. Phys. Lett. **79**(15), 2312–2314 (2001).
23. N. Carlsson, N. Ikeda, Y. Sugimoto, K. Asakawa, T. Takemori, Y. Katayama, N. Kawai, and K. Inoue, "Design, nano-fabrication and analysis of near-infrared 2D photonic crystal air-bridge structures," Opt. Quantum Electron. **34**, 123–131 (2002).
24. T. F. Krauss, R. M. DeLaRue, and S. Brand, "Two-dimensional photonic-bandgap structures operating at near infrared wavelengths," Nature **383**, 699–702 (1996).
25. S. Yamada, T. Koyama, Y. Katayama, N. Ikeda, Y. Sugimoto, K. Asakawa, N. Kawai, and K. Inoue, "Observation of light propagation in two-dimensional photonic crystal-based bent optical waveguides," J. Appl. Phys. **89**, 855–858 (2001).
26. A. Talneau, L. Le Gouezigou, and N. Bouadma, "Quantitative measurement of low propagation losses at 1.55 μm on planar photonic crystal waveguides," Opt. Lett. **26**, 1259–1261 (2001).
27. T. F. Krauss, "Patterned photonic crystal waveguides," in *Photonic Crystals and Light Localization in the 21st Century*, C. M. Soukoulis, ed. (Kluwer Academic, Dordrecht, The Netherlands, 2001), pp. 129–142.
28. D. Labilloy, H. Benisty, C. Weisbuch, T. F. Krauss, R. M. D. L. Rue, V. Bardinal, R. Houdré, U. Oesterle, D. Cassagne, and C. Jouanin, "Quantitative measurement of transmission, reflection, and diffraction of two-dimensional photonic band gap structures at near-infrared wavelengths," Phys. Rev. Lett. **79**, 4147–4150 (1997).
29. D. Labilloy, H. Benisty, C. Weisbuch, T. F. Krauss, D. Cassagne, C. Jouanin, R. Houdré, U. Oesterle, and V. Bardinal, "Diffraction efficiency and guided light control by two-dimensional photonic-bandgap lattices," IEEE J. Quantum Electron. **35**, 1045–1052 (1999).
30. B. D'Urso, O. Painter, J. O'Brien, T. Tombrello, A. Yariv, and A. Scherer, "Modal reflectivity in finite-depth two-dimensional photonic-crystal microcavities," J. Opt. Soc. Am. B **15**, 1155–1159 (1998).
31. M. Palamaru and P. Lalanne, "Photonic crystal waveguides: out-of-plane losses and adiabatic modal conversion," Appl. Phys. Lett. **78**, 1466–1468 (2001).
32. D. M. Atkin, P. S. J. Russell, T. A. Birks, and P. J. Robert, "Photonic band structure of guided Bloch modes in high index films fully etched through with periodic microstructure," J. Mod. Opt. **43**, 1035–1053 (1996).
33. The slope of the curve in Fig. 7 of Ref. 16.
34. M. Qiu, B. Jaskorzynska, M. Swillo, and H. Benisty, "Time-domain 2D modeling of slab-waveguide based photonic-crystal devices in the presence of out-of-plane radiation losses," Microwave Opt. Technol. Lett. **34**, 387–393 (2002).
35. Given a refractive-index contrast of $n_{\mathrm{guide}}/n_{\mathrm{air}} = 3$, the average optical path of the guided wave inside the air holes is less than 10% for $f \leqslant 0.30$.
36. M. Plihal and A. A. Maradudin, "Photonic band structure of two-dimensional systems: the triangular lattice," Phys. Rev. B **44**, 8565–8571 (1991).

37. H. Rigneault and S. Monneret, "Modal analysis of spontaneous emission in a planar microcavity," Phys. Rev. A **54**, 2356–2368 (1996).
38. L. C. Andreani and M. Agio, "Photonic bands and gap maps in a photonic crystal slab," IEEE J. Quantum Electron. **38**, 891–898 (2002).
39. D. J. Ripin, K. Y. Lim, G. S. Petrich, P. R. Villeneuve, S. H. Fan, E. R. Thoen, J. D. Joannopoulos, E. P. Ippen, and L. A. Kolodziejski, "One-dimensional photonic bandgap microcavities for strong optical confinement in GaAs and GaAs/Al_xO_y semiconductor waveguides," J. Lightwave Technol. **17**, 2152–2160 (1999).
40. J. Moosburger, M. Kamp, A. Forchel, R. Ferrini, D. Leuenberger, R. Houdré, S. Anand, and J. Berggren, "Nanofabrication of high quality photonic crystals for integrated optics circuits," Nanotechnology **13**, 341–345 (2002).
41. M. Qiu and S. L. He, "Numerical method for computing defect modes in two-dimensional photonic crystals with dielectric or metallic inclusions," Phys. Rev. B **61**, 12871–12876 (2000).
42. M. Qiu and S. L. He, "A nonorthogonal finite-difference time-domain method for computing the band structure of a two-dimensional photonic crystal with dielectric and metallic inclusions," J. Appl. Phys. **87**, 8268–8275 (2000).
43. M. Qiu and S. L. He, "Guided modes in a two-dimensional metallic photonic crystal waveguide," Phys. Lett. A **266**, 425–429 (2000).
44. M. Qiu and S. L. He, "FDTD algorithm for computing the off-plane band structure in a two-dimensional photonic crystal with dielectric or metallic inclusions," Phys. Lett. A **278**, 348–354 (2001).
45. The effective air fill factor value obtained from the fit is checked to fall within the range set by the SEM analysis that is influenced by the local hole shape fluctuations that are due to sample preparation, by the average on a limited number of holes, and by the cylindroconical hole shape.